RESEARCH   **Open Access**

A theoretical mesh-free scheme to model viscous drop interactions: a particle-based method

Alejandro Acevedo-Malavé

Abstract

Here a Lagrangian mesh-free formalism is presented to simulate the coalescence process between three unequal-sized liquid drops in the three-dimensional space. The surface tension forces acting on the surface of the drops cause the formation of a circular flat section when the droplets collide. The effect of polydispersity on the collision dynamics is simulated using a set of droplets with radius around 30 μm. It is important to see that the inhomogeneous distribution of the droplets size results in very important changes on the drops dynamics. The smoothed particle hydrodynamics scheme proposed here can be used to model situations where a continuum phase is included in the problem. The velocity vector fields are computed for each situation, and it can be seen that in the zone of contact between the droplets, there is an increment of the velocity value. This is due to the pressure distribution inside the drops.

Keywords: Fluid dynamics; Hydrodynamics; Drops; Coalescence; Navier-Stokes equation; Numerical method; SPH

Introduction

In the literature, many studies have been proposed for the numerical simulation of the coalescence and break up of droplets. The authors propose different methods to approach the dynamics of liquid drops by a numerical integration of the Navier-Stokes equations. These examine the motion of droplets and the dynamics that it follows in time and study the liquid bridge that arises when two drops collide. The effects of parameters such as Reynolds number, impact velocity, drop size ratio, and internal circulation are investigated, and different regimes for droplets collisions are simulated. In some cases, those calculations yield results corresponding to the four regimes of binary collisions: bouncing, coalescence, reflexive separation, and stretching separation. These numerical simulations suggest that the collisions that lead to rebound between the drops are governed by macroscopic dynamics. In these simulations the mechanism of formation of satellite drops was also studied, confirming that the principal cause of the formation of satellite drops is the 'end pinching,' while the capillary wave instabilities are the dominant feature in cases where a large value of the parameter impact is employed.

In this work the smoothed particle hydrodynamics (SPH) method is applied to simulate for the first time in three-dimensional space the hydrodynamic coalescence collision of three liquid drops in a vacuum environment. This method is employed in order to obtain the approximate numerical solutions of the equations of fluid dynamics by replacing the fluid with a set of particles. These particles may be interpreted as corresponding to the interpolation points from which properties of the fluid can be determined. Each SPH particle can be considered as a system of smaller particles. The SPH method is particularly useful when the fluid motion produces big deformations and a large velocity of the whole fluid.

A brief review of previous studies

Rekvig and Frenkel [1] reported a molecular simulation study of the mechanism of droplets covered with a surfactant monolayer coalesce. The authors proposed a model system where the rate-limiting step in coalescence is the rupture of the surfactant film. For this numerical study, one made use of the dissipative particle dynamics method using a coarse-grained description of the oil, water, and surfactant molecules. The authors found that the rupture rate is highest when the surfactant has a negative natural curvature, lowest when it has a zero natural curvature, and lying in between when it has a

Correspondence: alaceved@ivic.gob.ve
Centro Multidisciplinario de Ciencias, Instituto Venezolano de Investigaciones Científicas (IVIC), Mérida 5101, Venezuela

positive natural curvature. Gokhale et al. [2] studied the coalescence of two condensing drops and the shape evolution of the coalesced drops. Image analyzing interferometry is used to study the coalescence of two drops of 2-propanol, and the shape evolution after the coalescence is found to be driven by the capillary forces inside the drop.

Foote [3] proposed a method to study the dynamics of liquid drops by a numerical integration of the Navier-Stokes equations. This author examined the motion of droplets with the application to the raindrop problem. The study was restricted to the collision of equal-sized drops along their line of centers. Numerical solutions were developed to study the rebound of water droplets in air. It is found that except for a small viscous effect, the Weber number of the drops determines the dynamics of the collision and the bounce time. Decent et al. [4] studied the formation of a liquid bridge during the coalescence of droplets. In this paper, the authors considered a mathematical model where the pressure singularity is removed at the instant of the impact for the coalescence of two viscous liquid volumes in an inviscid gas or in a vacuum environment. The formation of the liquid bridge is examined for two cases: (a) two infinitely long liquid cylinders, and (b) two coalescing spheres. In both cases the numerical solutions are calculated for the velocity and pressure fields, and the removal of the pressure singularity is confirmed.

Mohamed-Kassim and Longmire [5] conducted particle image velocimetry (PIV) experiments to study the coalescence of single drops through planar liquid/liquid interfaces. Sequences of velocity vector fields were obtained with a high-speed video camera and the subsequent PIV analysis. Two ambient liquids with different viscosities but similar densities were examined. After rupture, the free edge of the thin film receded rapidly, allowing the drop fluid to sink into the bulk liquid below. The vorticity generated in the collapsing fluid developed into a vortex ring, straddling the upper drop surface. The inertia of the collapse deflected the interface downward before it rebounded upward. During this time, the vortex core split so that part of its initial vorticity moved inside the drop fluid while part of it remained in the ambient fluid above it. The velocity of the receding free edge was smaller for higher ambient viscosity, and the pinching of the upper drop surface caused by the shrinking capillary ring wave was stronger when the ambient viscosity was lower. This resulted in a higher maximum collapse speed and higher vorticity values in the dominant vortex ring.

Qian and Law [6] proposed an experimental investigation of binary collision of drops with emphasis on the transition between different regimes, which may be obtained as an outcome of the collision between droplets. In this study the authors analyzed the results using photographic images, which show the evolution of the dynamics exhibited for different values of the Weber number. As a result of the experiment reported by Qian and Law [6], five different regimes governing the collision between droplets are proposed: (a) coalescence after a small deformation, (b) bouncing, (c) coalescence after substantial deformation, (d) coalescence followed by separation for head-on collisions, and (e) coalescence followed by separation for off-center collisions. Ashgriz and Poo [7] conducted an experimental study of the binary collision of water droplets for a wide range of Weber numbers and impact parameters. These authors identified two types of collisions leading to the drops separation, which can be reflexive separation and stretching separation. It is found that the reflexive separation occurs in head-on collisions, while stretching separation occurs in high values of the impact parameter. Experimentally, the authors reported the border between the two types of separation and also collisions that lead to coalescence.

Narsimhan [8] proposed a model for drop coalescence in a turbulent flow field as a two-step process consisting in the formation of a doublet due to drop collisions followed by coalescence of the individual droplets occurring after the drainage of the intervening film by the action of van der Waals, electrostatic, and random turbulent forces. The turbulent flow field was assumed to be locally isotropic. A first-passage-time analysis was employed for the random process in the intervening continuous phase film between the two drops. The first two moments of coalescence time distribution of the doublet were evaluated. The average drop coalescence time of the doublet was dependent on the barrier due to the net repulsive force. The predicted average drop coalescence time was found to decrease whenever the ratio of the average turbulent force to repulsive force barrier became larger. The calculated coalescence time distribution was broader with a higher standard deviation at lower energy dissipation rates, higher surface potentials, smaller drop sizes, and smaller size ratios of unequal drop pairs. Zhang et al. [9] conducted a study on coalescence of unequal-sized drops. In this study the coalescence of a drop with a flat liquid surface pinches off a satellite droplet from its top, whereas the coalescence of two equally sized drops does not appear to produce, in this case, a satellite drop. The authors found that the critical ratio grows monotonically with the Ohnesorge number and, as reported, the experimental coalescence of two unequal-sized droplets.

Yoon et al. [10] carried out a study about the coalescence of two equal-sized deformable drops in an axisymmetric flow using a boundary integral method. The thin film dynamics are simulated up to a film thickness of 10 to 4 times the non-deformed drop radius. The authors studied two different regimes for head-on collisions between the droplets. At lower capillary numbers, the interfaces of the

film between the drops remain in a circular flat form up to the film rupture. At higher capillary numbers, the film becomes dimpled at an early stage of the collision process; also, the rate of the film drainage slows down after the dimple formation. Mashayek et al. [11] studied the coalescence collision of two liquid drops using a Galerkin finite element method in conjunction with the spine-flux method for the free surface tracking. The effects of some parameters like Reynolds number, impact velocity, drop size ratio, and internal circulation on the coalescence process were investigated. The long-time oscillations of the coalesced drops and the collision of unequal-sized liquid drops were studied to illustrate the liquid mixing during the collision. Aarts et al. [12] proposed a study of droplet coalescence in a molecular system with a variable viscosity and a colloid-polymer mixture with an ultra-low surface tension. When either the viscosity is large or the surface tension is small enough, one can observe that the opening of the liquid bridge initially proceeds at a constant speed set by the capillary velocity. In the first system studied, one finds that the inertial effects become dominant at a Reynolds number of about 1.5, and the neck then grows as the square root of time. In the second system, one finds that decreasing the surface tension by a factor of 105 opens the way to a more complete understanding of the hydrodynamics involved. Thoroddsen et al. [13] conducted an experimental study of surface profiles and propagation of Marangoni waves along the surface of a drop. One finds that the capillary-Marangoni waves along the water drop show self-similar character when measured in terms of the arc length of the original surface. The coalescence for different liquids is also studied, finding that the coalescence velocity of a water drop with a more viscous liquid is nearly independent of the viscosity difference strength.

Cristini et al. [14] proposed an algorithm for the adaptive restructuring of meshes on the evolving surfaces. The resulting discretization depends on the instantaneous configuration of the surface. As an application of the adaptive discretization algorithm, some simulations of the drop breakup and coalescence were presented. The results show that the algorithm can accurately resolve detailed features of the deformed fluid interfaces and the slender filaments of the drop breakup as well as dimpled regions with drop coalescence. Wang et al. [15] studied the effect of glycerol on the coalescence of water drops in stagnant oil phase. In this reference the authors considered the binary coalescence of water drops formed through capillaries at low inlet flow rates in an immiscible stagnant oil phase. The evolution of the coalescence process is shown in this case. Sun et al. [16] conducted a study of deformation and mass transfer for binary droplet collisions with the moving particle semi-implicit method. A surface tension model is implemented in numerical simulations to study large deformation processes and a mechanism map is reported to distinguish different collisions regimes.

Xing et al. [17] put forward a lattice Boltzmann method-based-single-phase free surface model to study the interfacial dynamics of coalescence, droplet formation, and detachment phenomena related to surface tension and wetting effects. A perturbation similar to the first step in Gunstensen's color model is added to the distribution functions of the interface cells in order to incorporate the surface tension into the single-phase model. Implementations of the model are verified by simulating the processes of droplet coalescence, droplet formation, and detachment from ceiling and from nozzles with different shapes and different wall wetting properties.

Jia et al. [18] proposed a lattice Boltzmann simulation for collisions between two liquid drops in an immiscible liquid in a linear Stokes flow. The results reported in this reference were compared to the experimental results and the asymptotic solutions. The mixing of a contaminant that is initially contained in one of the drops is discussed and compared to the results of particle tracking simulations. In this study Jia et al. [18] verified that the Oxford approach of the lattice Boltzmann method can be used to perform useful simulations of drop coalescence in which the mixing of a chemical contaminant that is initially confined to one of the drops occurs. The lattice Boltzmann method solutions were compared with analytical results. The most significant finding was that after the coalescence of a pure drop with a contaminated drop, the contaminant is initially confined to half of the product drop. The results for mixing subsequent to coalescence are in agreement with the results obtained from tracking marker particles in the exact flow field for a spherical drop in a shear flow. The simulations with marker particles suggest that mixing occurs more rapidly in drops with much smaller viscosities than the suspending medium and that diffusion is the dominant mechanism of mixing for Schmidt numbers smaller than about 50. For larger values the dimensionless mixing time is relatively insensitive to the Schmidt number.

Wu et al. [19] reported experimental results on the coalescence of two liquid drops driven by surface tension. Using a high-speed imaging system, the authors studied the early-time evolution of the liquid bridge that is formed upon the initial contact of two liquid drops in air. It is found that the liquid bridge radius follows the scaling law in the inertial regime. Further experiments demonstrate that such scaling law is robust when using fluids of different viscosities and surface tensions. The dimensionless pre-factor is measured to be in the range of 1.03 to 1.29, which is lower than the pre-factor 1.62 predicted by the numerical simulation of Duchemin et al. [20] for inviscid drop coalescence.

Colagrossi and Landrini [21] put forward an SPH formulation for the simulation of interfacial flows, that is, flow fields of different fluids separated by interfaces. The scheme proposed for the simulation of interfacial flows starts considering that the fluid field is represented by a collection of N particles interacting with each other according to evolution equations of the general form

$$\frac{d\rho_i}{dt} = -\rho_i \sum_j M_{ij},$$
$$\frac{d\mathbf{u}_i}{dt} = -\frac{1}{\rho_i} \sum_j F_{ij} + f_i, \qquad (1)$$
$$\frac{d\mathbf{x}_i}{dt} = \mathbf{u}_i.$$

The terms M_{ij} and F_{ij} arise from the mass and momentum conservation equations. In the Equation 1, the density ρ_i, the velocity $\mathbf{u}_i$ of the particles, and the force f_i which can be any body force appear. When there are fluid regions with a sharp density gradient (interfaces), the SPH standard formulations must be modified in order to be applied to treat such systems. This difficulty can be circumvented using the following discrete approximations

$$\text{div}(\mathbf{u}_i) = \sum_j (\mathbf{u}_j - \mathbf{u}_i) \cdot \nabla W_{ji} \frac{m_j}{\rho_j},$$
$$\nabla A_i = \sum_j (A_j - A_i) \nabla W_{ji} \frac{m_j}{\rho_j}. \qquad (2)$$

Here W is the kernel or smoothing function and A can be any scalar field or continuous function. The small difference between the Equation 2 and the standard equation that uses m_j/ρ_i instead m_j/ρ_j is important for the treatment of the case of small density ratios. On the other hand, it can be shown that the pressure gradient can be written as

$$\nabla p_i = \sum_j (p_j + p_i) \nabla W_{ji} dV_j. \qquad (3)$$

Equation 3 is variationally consistent with Equation 2. In this scheme the terms M_{ij} and F_{ij} appearing in Equation 1 are given by the expressions

$$M_{ij} = (u_j - u_i) \cdot \nabla W_{ji} \frac{m_j}{\rho_j},$$
$$F_{ij} = (p_j + p_i) \nabla W_{ji} \frac{m_j}{\rho_j}. \qquad (4)$$

A density re-initialization is needed when each particle has a fixed mass; and when the number of particles is

constant, the mass conservation is satisfied. Yet if one uses Equation 1 for the density, the consistency between mass, density, and occupied area is not satisfied. To solve this problem, the density is periodically re-initialized applying the expression

$$\rho_i = \sum_j m_j W_{ij}. \qquad (5)$$

In this formulation special attention must be paid to the kernel. In fact, depending on which kernel is used, Equation 5 could introduce additional errors. For this reason, a first-order interpolation scheme is suitable to re-initialize the density field by using the equation

$$\langle \rho_i \rangle = \sum_j \rho_j W_j^{\text{MLS}}(x_i) dV_j = \sum_j m_j W_j^{\text{MLS}}(x_i), \qquad (6)$$

where W_j^{MLS} is the moving least-square kernel.

The XSPH (extended smoothed particle hydrodynamics, which is a variant of the SPH method for the modeling of free surface flows) velocity correction Δu_i is introduced to prevent particles inter-penetration, which takes into account the velocity of the neighbor particles using a mean value of the velocity, according to the equations

$$\langle \mathbf{u}_i \rangle = u_i + \Delta u_i, \quad \Delta u_i = \frac{\varepsilon'}{2} \sum_j \frac{m_j}{\bar{\rho}_{ij}} (u_j - u_i) W_{ji}, \qquad (7)$$

Where $\bar{\rho}_{ij}$ is the mean value of density between the ith and jth particle, and ε' is the relative change of an arbitrary quantity between simulations. Morris [22] proposes a method for the simulation of two-phase flows including surface tension forces. The approach is based on the SPH formalism. Due to the full Lagrangian features of the SPH method that maintains fluid-fluid interfaces without employing high-order advection schemes, several possible implementations of surface tension force are suggested in this reference. The author-made comparisons with a grid-based volume of fluid method for two-dimensional flows are excellent. The methods presented by Morris [22] apply to problems involving interfaces of arbitrary shape undergoing fragmentation and coalescence within a two-phase system.

Hu and Adams [23] proposed a multi-phase SPH method for both macroscopic and mesoscopic flows. In this reference the particle-averaged spatial derivative approximations are derived from a particle smoothing function in which the neighboring particles only contribute to the specific volume; this method handles

density discontinuities across phase interfaces naturally. The newly formulated viscous terms allow for a discontinuous viscosity and ensure continuity of velocity and shear stress across the phase interface. Based on this formulation, thermal fluctuations are introduced in a straightforward way. A new simple algorithm is proposed. Adami et al. [24] proposed a conservative method for the simulation of multi-phase flows with surfactant. The effects of the surface tension active substances are included by a scalar quantity describing the local concentration of molecules in the bulk phase and on the interface. This method can simulate insoluble surfactant on an arbitrary interface geometry as well as interfacial transport such as adsorption or desorption. The flow field dynamics and the surfactant dynamics are coupled through a constitutive equation, which relates the local surfactant concentration to the local surface tension coefficient. Hence, the surface tension model includes capillary and Marangoni forces. Hu and Adams [25] also proposed an incompressible multi-phase SPH method. A fractional time step method is introduced to enforce both the zero-density-variation condition and the velocity-divergence-free condition at each full time step. To obtain sharp density and viscosity discontinuities in an incompressible multi-phase flow, a new multi-phase projection formulation, in which the discretized gradient and divergence operators do not require a differentiable density or viscosity field, is proposed in [25]. A constant density approach for incompressible multi-phase SPH simulations was introduced by Hu and Adams [26], which corrects ([25]) intermediate density errors by adjusting the half-time-step velocity with exact projection.

Adami et al. [27] proposed a new surface tension formalism in the framework of the smoothed particle hydrodynamics scheme to simulate multi-phase flows. To obtain a stable and accurate scheme for surface curvature, a divergence approximation is derived. Furthermore, the authors introduce a density-weighted color-gradient formulation to reflect the reality of an asymmetrically distributed surface tension force. This formulation can handle phase interfaces with density and viscosity ratios of up to 1,000 and 100, respectively. Acevedo-Malavé and García-Sucre [28-31] applied the SPH method to model for the first time the hydrodynamical coalescence collisions of two and many droplets in vacuum environment. In these studies the authors reported the formation of clusters of equal-size drops, where the effect of the surface tension arises due to the formation of flocs. It can be seen that the smoothing function used here was the cubic B-spline kernel [32], and the equation of the state considered was a general Mie-Gruneisen form of EOS for water drops.

Numerical details

The smoothed particle hydrodynamics formalism

Smoothed particle hydrodynamics is a method to solve approximately the equations of fluid dynamics, replacing the fluid by a set of particles. The SPH method was simultaneously invented by Lucy [33] and Gingold and Monaghan [34] to solve astrophysical problems.

In the SPH model, the fluid is represented by a discrete set of N particles. The position of the ith particle is denoted by the vector $\mathbf{r}_i$, $i = 1, \ldots, N$. The SPH scheme is based on the idea that a smoothed representation $A_s(\mathbf{r})$ of the continuous function $A(\mathbf{r})$ can be obtained from the convolution integral

$$A_s(\mathbf{r}) = \int A(\mathbf{r}')W(\mathbf{r}-\mathbf{r}', \boldsymbol{h})d\mathbf{r}'. \tag{8}$$

Here h is the smoothing length, and the smoothing function W satisfies the normalization condition

$$\int W(\mathbf{r}-\mathbf{r}', \boldsymbol{h})d\mathbf{r}' = 1. \tag{9}$$

The integration is performed over all spaces. In the limit of h tending to 0, the smoothing function W becomes a Dirac delta function, and the smoothed representation $A_s(\mathbf{r})$ tends to $A(\mathbf{r})$.

In the SPH scheme, the properties associated with particle i are calculated by approximating the integral in Equation 8 by the sum

$$\begin{aligned} A_i &= \sum_j \Delta V_j A_j W(\mathbf{r}_i-\mathbf{r}_j, h) \\ &= \sum_j m_j \frac{A_j}{\rho_j} W(\mathbf{r}_i-\mathbf{r}_j, h). \end{aligned} \tag{10}$$

Here ΔV_j is the fluid volume associated with particle j, and m_j, and ρ_j are the mass and density of the jth particle, respectively. In the above sum, A_j is the value of a physical field $A(\mathbf{r})$ in the particle j, and the sum is performed over all particles. Furthermore, the gradient of A is calculated using the expression

$$\nabla A_i = \sum_j m_j \frac{A_j}{\rho_j} \nabla_i W(\mathbf{r}_i-\mathbf{r}_j, h). \tag{11}$$

In the Equation 10, ρ_i/m_i can be replaced by the particle number density $n_i = \rho_i/m_i$ so that

$$A_i = \sum_j \frac{A_j}{n_j} W(\mathbf{r}_i-\mathbf{r}_j, h). \tag{12}$$

The particle number density can be calculated using the expression

$$n_i = \sum_j W(\mathbf{r}_i-\mathbf{r}_j, h), \tag{13}$$

and the mass density is given by

$$\rho_i = \sum_j m_j W(\mathbf{r}_i-\mathbf{r}_j, h). \tag{14}$$

Similarly, the gradient can be calculated using the expression

$$\nabla A_i = \sum_j \frac{A_j}{\boldsymbol{n}_j} \nabla_i W\left(\mathbf{r}_i - \mathbf{r}_j, h\right). \tag{15}$$

The velocity and acceleration fields are given by [28]

$$\frac{d\mathbf{r}_i}{dt} = \mathbf{v}_i,$$
$$\frac{d\mathbf{v}_i^\alpha}{dt} = \sum_{j=1}^{N} m_j \left(\frac{\sigma_i^{\alpha\beta}}{\rho_i^2} + \frac{\sigma_j^{\alpha\beta}}{\rho_j^2} \right) \cdot \nabla W_{ij}^h, \tag{16}$$

where σ is the total stress tensor.

The internal energy evolution is given by the expression [28]

$$\frac{dE_i}{dt} = \frac{1}{2} \sum_{j=1}^{N} m_j \left(\frac{p_i}{\rho_i^2} + \frac{p_j}{\rho_j^2} \right) \left(v_i^\beta - v_j^\beta \right) \frac{\partial W_{ij}}{\partial x_i^\beta} + \frac{\mu_i}{2\rho_i} \varepsilon_i^{\alpha\beta} \varepsilon_i^{\alpha\beta}, \tag{17}$$

In the above equation, p is the pressure, μ is the dynamic viscosity, and ε is the shear strain rate.

In the present work, the model is performed in three dimensions and the cubic B-spline kernel is used [32]. In this paper, water drops are considered and the equation of state in the hydrodynamical code was a general Mie-Gruneisen form of equation of state with different analytic forms for states of compression $(\rho/\rho0\text{-}1) > 0$ and tension $(\rho/\rho0\text{-}1) < 0$ [28].

This equation has several parameters, namely, the density ρ, the reference density ρ_0, and the constants A_1, A_2, A_3, C_1, and C_2. This equation of state defines the pressure P as

$$P = A_1 \left(\frac{\rho}{\rho_0} - 1 \right) + A_2 \left(\frac{\rho}{\rho_0} - 1 \right)^2$$
$$+ A_3 \left(\frac{\rho}{\rho_0} - 1 \right)^3 \quad \text{if} \quad \left(\frac{\rho}{\rho_0} - 1 \right) > 0 \tag{18}$$

and

$$P = C_1 \left(\frac{\rho}{\rho_0} - 1 \right) + C_2 \left(\frac{\rho}{\rho_0} - 1 \right) \quad \text{if} \quad \left(\frac{\rho}{\rho_0} - 1 \right) < 0. \tag{19}$$

In all calculations the following values are used for the constants: $A_1 = 2.20 \times 10^6$ kPa, $A_2 = 9.54 \times 10^6$ kPa, $A_3 = 1.46 \times 10^7$ kPa, $C_1 = 2.20 \times 10^6$ kPa, $C_2 = 0.00$ kPa, and $\rho_0 = 1,000.0$ kg/m^3.

The convergence of the SPH method

The convergence of the smoothed particle hydrodynamics method can be proved if one follows the conjectures of Di Lisio et al. [35]. Theorems 1 and 2 of [35] can be directly applied to show the convergence of the sequence of empirical measures $\{\mu_N(t)\}_{N = 1,2, \ldots}$, whose evolution is stated, for any N, by the equations of motion of the SPH scheme, to the solution of the problem as $N \to \infty$. If the points x_i are independent identically distributed random variables of probability μ, then the empirical measures

$$\nu_N = \frac{1}{N} \sum_{i=1}^{N} \delta_{xi}, \quad N = 1, 2, \ldots \tag{20}$$

converge to the measure μ, that is, for any measurable bounded function

$$f : \int \nu_N(dx) f(x) \xrightarrow{N \to \infty} \int \mu(dx) f(x), \tag{21}$$

for suitable sequences $x_1, x_2, \ldots, x_m, \ldots$.

If one considers the quantity

$$\left(\int \nu_N(dx) f(x) - \int \mu(dx) f(x) \right)^2, \tag{22}$$

its expectation value gives

$$\int \left(\frac{1}{N} \sum_i f(x_i) - \int \mu(dx) f(x) \right)^2 \mu(dx_1) \ldots \mu(dx_N)$$
$$= \frac{1}{N} \left[\int f^2(x) \mu(dx) - \left(\int f(x) \mu(dx) \right)^2 \right]. \tag{23}$$

The quantity in the square brackets is bounded and the expectation value goes to 0 as $N \to \infty$. This means that for almost all the sequences of initial conditions, the empirical measures converge to the measure μ_0, as $N \to \infty$ [35].

Results and discussion

Numerical simulation of the coalescence phenomenon between unequal-sized liquid drops

In order to simulate the hydrodynamical coalescence collisions between three unequal-sized water drops, the smoothed particle hydrodynamics formalism has been employed. Inside the SPH code were defined drops with 10, 16, and 30 μm of diameter and 26,656 SPH particles for the three drops with a collision velocity of 15.0 mm/ms directed to the center of the coordinate system.
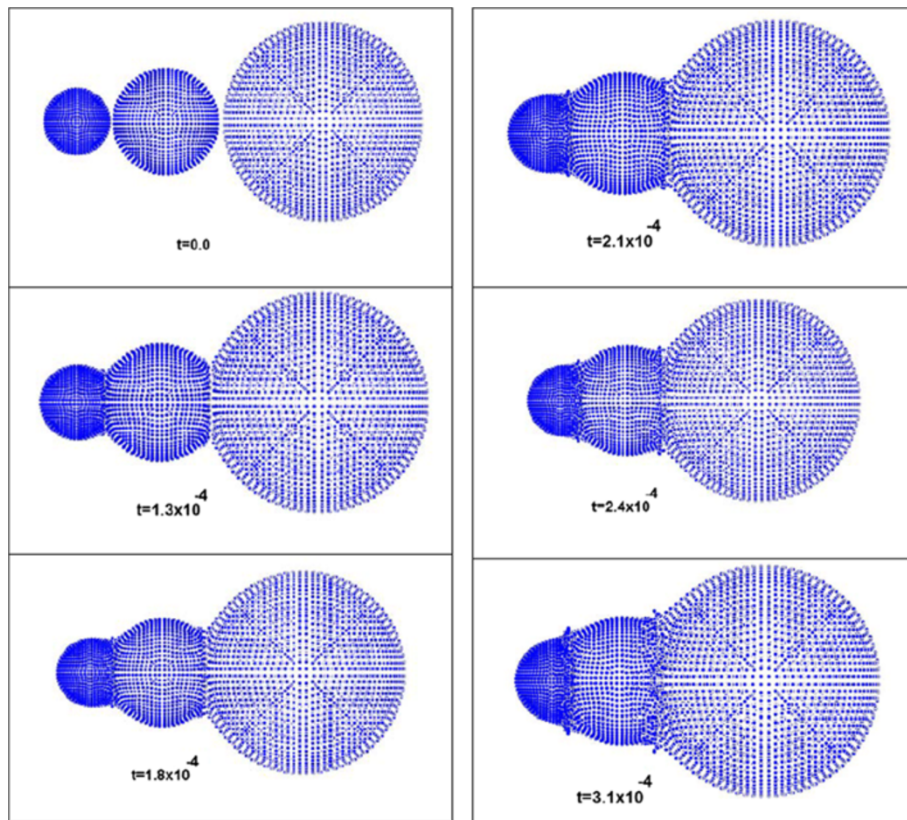
Figure 1 Sequence of times showing the evolution of the collision between three drops (permanent coalescence). The evolution of time is given in milliseconds; V_{col} = 15.0 mm/ms.
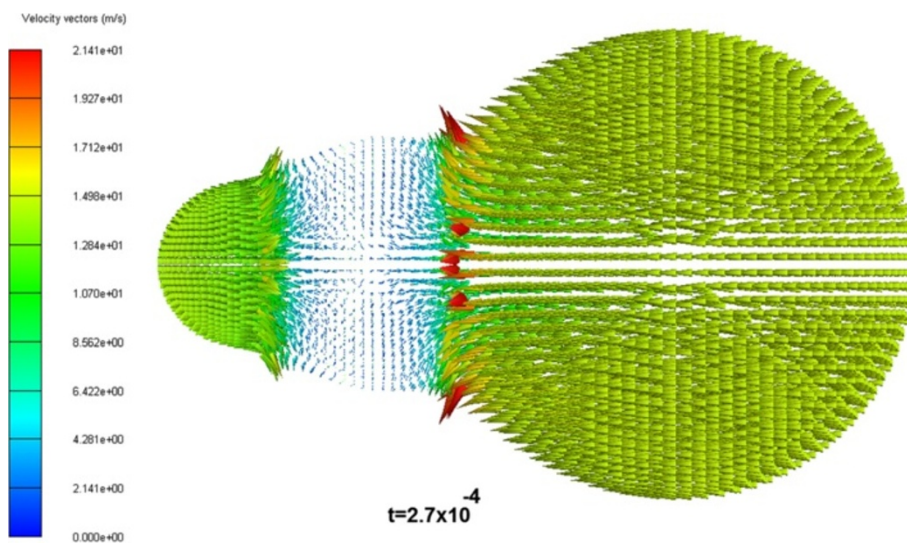

Figure 2 Velocity vector field for collision between three drops at t = 2.7 × 10^{-4} ms (permanent coalescence). The evolution time is given in milliseconds; V_{col} = 15.0 mm/ms.
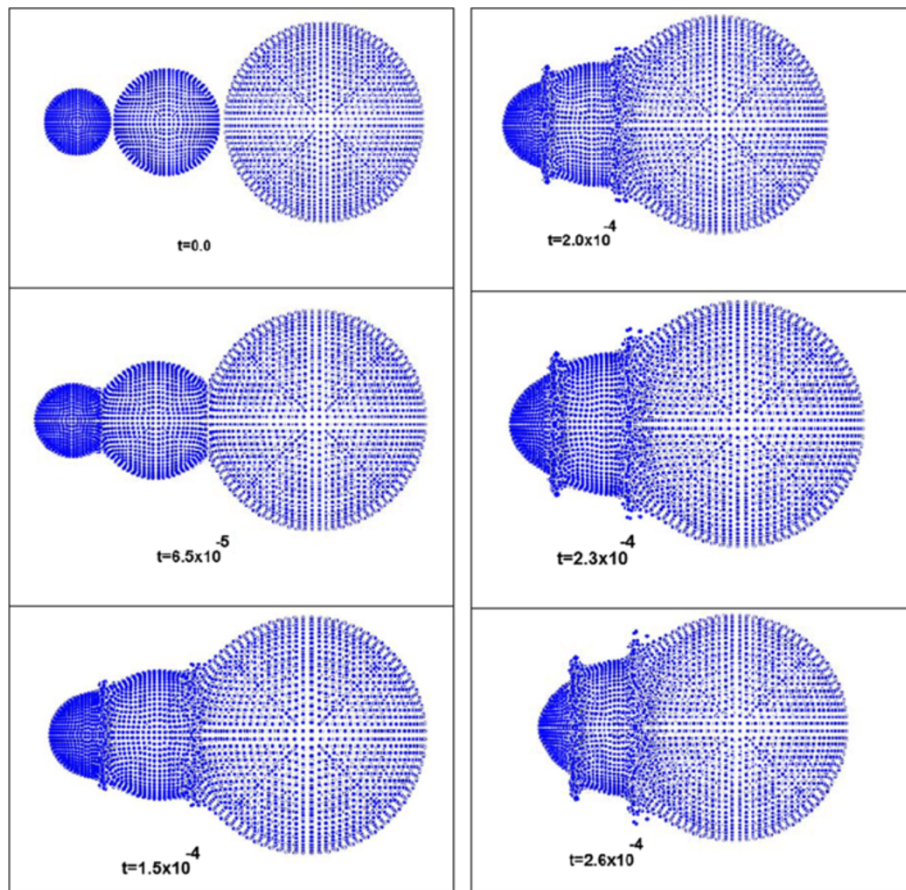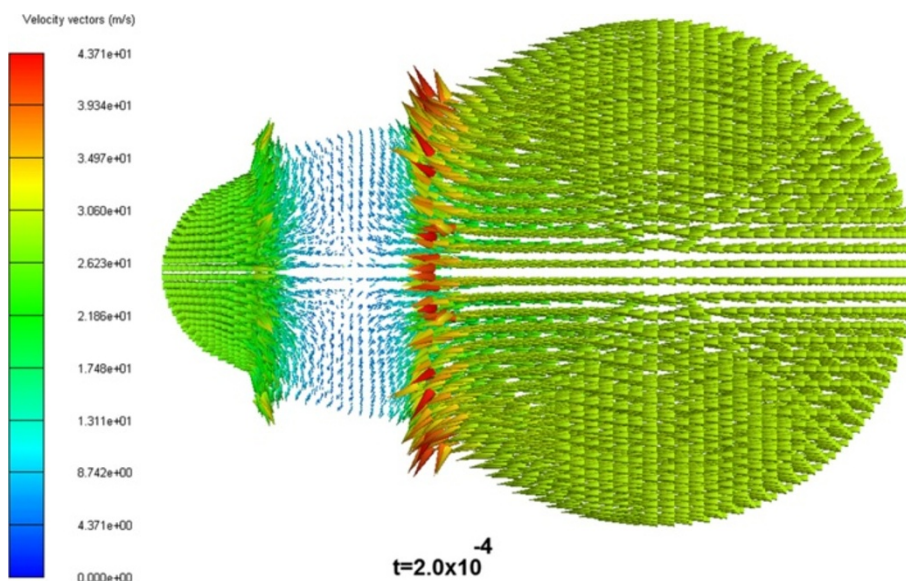
Figure 3 Sequence of times showing the evolution of the collision between three drops (fragmentation). The evolution of time is given in milliseconds; V_{col} = 30.0 mm/ms.

Figure 4 Velocity vector field for the collision between three drops at $t = 2.0 \times 10^{-4}$ ms (fragmentation). The evolution time is given in milliseconds; V_{col} = 30.0 mm/ms.
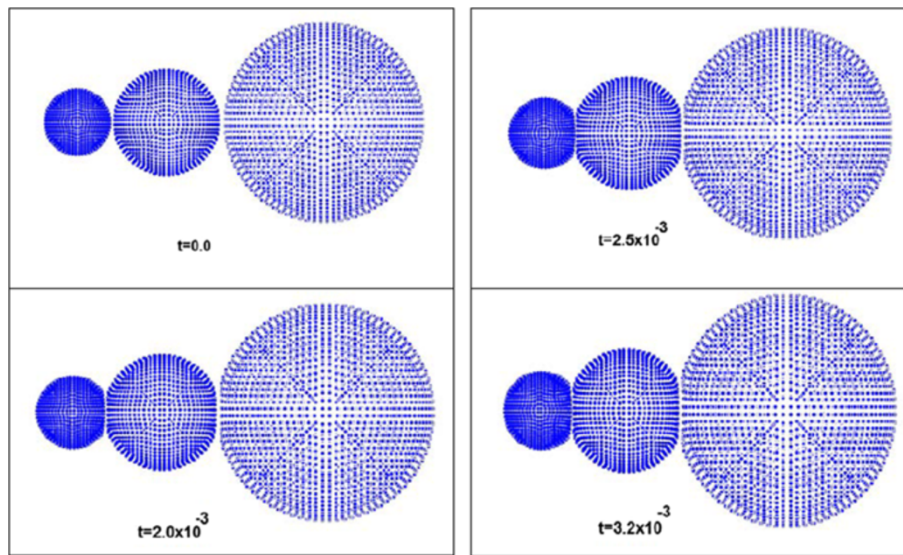
Figure 5 Sequence of times showing the evolution of the collision between three drops with V_{col} = 0.5 mm/ms. The evolution of time is given in milliseconds.

It can be seen in Figure 1 that at $t = 1.3 \times 10^{-4}$ ms, a flat circular section appears, which increases its diameter as dynamics progresses. It is observed in the dynamics that at $t = 1.8 \times 10^{-4}$ ms, a bridge structure between the drops appears in the region of contact, which disappears at a later time due to the penetration of SPH particles between the drops. Figure 2 shows the velocity vector field inside the droplets as well as in the region of contact between them at $t = 2.7 \times 10^{-4}$ ms. It is important to see that inside the drops, the fluid tends to have a velocity value around

the initial velocity of 12.00 mm/ms, while in the area of contact between the drops, an increase in the fluid velocity to a value of 17.0 mm/ms is observed.

The outcomes reported by Qian and Law [6] are in good agreement with this results; in fact, the experimental study of these authors shows a similar scenario when two drops approach each other (see Figure four (a) of reference [6]). In this SPH calculation, the relative velocity is not enough to produce fragmentation of the drops and subsequently to produce small satellite droplets. In this calculation, the
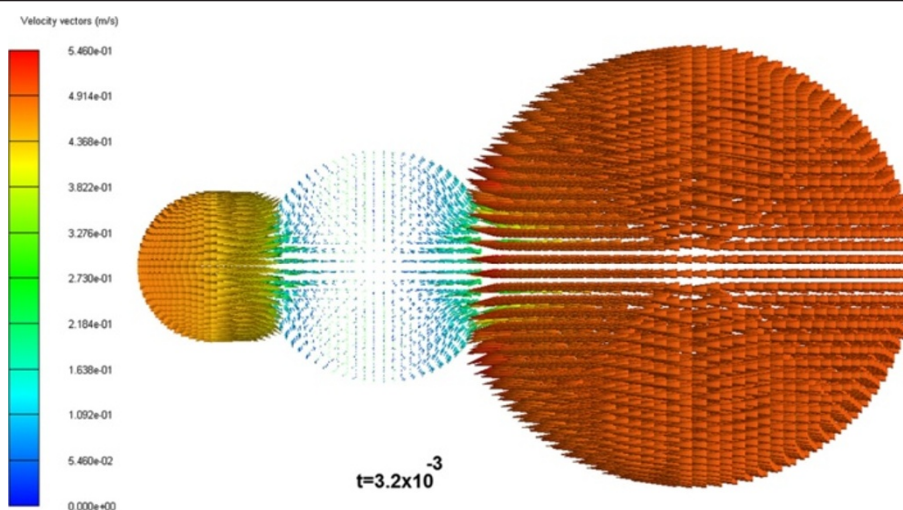

Figure 6 Velocity vector field for the collision between three drops at $t = 3.2 \times 10^{-3}$ ms. The evolution time is given in milliseconds; V_{col} = 0.5 mm/ms.

coalescence is permanent and the resulting deformed drop reaches the equilibrium. On the other hand, the experiments of Qian and Law [6] do not have a sufficient resolution to show in detail the deformation of the drops just before the formation of the bridge. However, the appearance of the flat circular section shown in Figure 1 is in good agreement with the experimental and theoretical outcomes reported in the literature [36-40].

In order to simulate the fragmentation phenomenon, inside the SPH code were defined drops with 10, 16, and 30 μm of diameter and 26,656 SPH particles for the three drops with a collision velocity of 30.0 mm/ms directed to the center of the coordinate system. With this value for the velocity of collision, it is observed that the fragmentation phenomenon arises. In the first stage of the calculation at $t = 6.5 \times 10^{-5}$ ms, the collision of the three droplets is shown in Figure 3. After this slide, a wave front can be seen traveling at the zone of interaction between the drops until at 2.6×10^{-4} ms, which is the time where the dynamic was stopped. Figure 4 shows the velocity vector field after the fragmentation of the drops has taken place. As shown in Figure 4, the fluid velocity inside the drops is 27 mm/ms, which is less than the initial rate of collision, while the fluid that is spread to the edges is accelerated reaching a speed of 35.0 mm/ms. A longer stretched ligament is produced between the drops, and the amount of satellite droplets increases with the evolution of dynamics. Figure 3 illustrates that a small portion of the fluid begins to separate, stretching away from the bigger drop, and a nonuniform pressure field is created inside the ligament. This is related to the value in the velocity vector field differences [22].

Flocculation occurs when the collision velocity is decreased below the range corresponding to permanent coalescence. These calculations were performed for droplets with 10, 16, and 30 μm of diameter and 26,656 SPH particles for the three drops with a collision velocity of 0.5 mm/ms directed to the center of the coordinate system. At the beginning of the calculation, it can be observed at $t = 2.0 \times 10^{-3}$ ms (see Figure 5) that a flat circular section appears between the three droplets. It can be seen in this calculation that the surface tension forces prevailing and the inertial forces are of secondary importance. As the dynamics run, a stretching of the surface of the drops until $t = 3.2 \times 10^{-3}$ ms can be observed and the droplets form a floc. Figure 6 shows the velocity vector field at $t = 3.2 \times 10^{-3}$ ms in the flocculation process. As shown in Figure 6, the fluid velocity inside the drops is around 0.4 mm/ms and at the zone of contact of the droplets, the velocity is around 0.3 mm/ms.

Conclusions
An adequate methodology using the SPH method in three-dimensional space was presented for the calculation of hydrodynamics collisions. As a result of the collision between droplets, the formation of a flat circular section was obtained for a range of values of the collision velocity. This flat circular section appears due to the existence of surface tension forces acting on each droplet. Some possible outcomes for the collision process were found: coalescence, fragmentation, and flocculation of liquid drops. The velocity vector fields were constructed for the different cases. It can be seen that the fluid inside the drops tends to accelerate the SPH particles at the zone of contact between the droplets. This behavior is due to the nonuniform pressure differential inside the drops. At the zone of the drops that have no interaction with any other drop, the fluid tends to diminish the internal velocity. This can be explained by the behavior of the pressure field inside the drops; in fact, in that zone of the droplets, the inhomogeneous pressure field has a minimal value.

Author's information
AAM received his PhD (2007) from the Venezuelan Institute for Scientific Research (IVIC), Venezuela in Physics: Fluid Mechanics. He is a researcher from IVIC in Venezuela. His main research interests are in the field of coalescence of liquid drops using the smoothed particle hydrodynamics (SPH) formalism.

References
1. Rekvig, L, Frenkel, D: Molecular simulations of droplet coalescence in oil/water/surfactant systems. J. Chem. Phys. **127**, 1–11 (2007)
2. Gokhale, SJ, Dasgupta, S, Plawsky, JL, Wayner, PC: Reflectivity-based evaluation of the coalescence of two condensing drops and shape evolution of the coalesced drop. Phys. Rev. E. **70**, 1–12 (2004)
3. Foote, GB: The water drop rebound problem: dynamics of collision. J. Atmos. Sci. **32**, 390–401 (1974)
4. Decent, SP, Sharpe, G, Shaw, AJ, Suckling, PM: The formation of a liquid bridge during the coalescence of drops. Int. J. Multi-phase Flow **32**, 717–738 (2006)
5. Mohamed-Kassim, Z, Longmire, EK: Drop coalescence through a liquid/liquid interface. Phys. Fluids **16**, 1–47 (2004)
6. Qian, J, Law, CK: Regimes of coalescence and separation in droplet collision. J. Fluid Mech. **331**, 59–80 (1997)
7. Ashgriz, N, Poo, JY: Coalescence and separation of binary collisions of liquid drops. J. Fluid Mech. **221**, 183–204 (1990)
8. Narsimhan, G: Model for drop coalescence in a locally isotropic turbulent flow field. J. Coll. Interf. Sci. **272**, 197–209 (2004)
9. Zhang, FH, Li, EQ, Thoroddsen, ST: Satellite formation during coalescence of unequal size drops. Phys. Rev. Lett. **102**, 1–4 (2009)
10. Yoon, Y, Baldessari, F, Ceniceros, HD, Leal, LG: Coalescence of two equal-sized deformable drops in an axisymmetric flow. Phys. Fluids **19**, 1–24 (2007)
11. Mashayek, F, Ashgriz, N, Minkowycz, WJ, Shotorban, B: Coalescence collision of liquid drops. Int. J. Heat Mass Trans. **46**, 77–89 (2003)
12. Aarts, D, Lekkerkerker, H, Guo, H, Wegdam, G, Bonn, D: Hydrodynamics of droplet coalescence. Phys. Rev. Lett. **95**, 1–11 (2005)
13. Thoroddsen, ST, Qian, B, Etoh, TG, Takehara, K: The initial coalescence of miscible drops. Phys. Fluids **19**, 1–21 (2007)

14. Cristini, V, Bawzdziewicz, J, Loewenberg, M: An adaptive mesh algorithm for evolving surfaces: simulations of drop breakup and coalescence. J. Comput. Phys. **168**, 445–463 (2001)
15. Wang, W, Gong, J, Ngan, KH, Angeli, P: Effect of glycerol on the binary coalescence of water drops in stagnant oil phase. Chem. Eng. Res. Design **87**, 1640–1648 (2009)
16. Sun, Z, Xi, G, Chen, X: Mechanism study of deformation and mass transfer for binary droplet collisions with particle method. Phys. Fluids **21**, 1–13 (2009)
17. Xing, XQ, Butler, DL, Ng, SH, Wang, Z, Danyluk, S, Yang, C: Simulation of droplet formation and coalescence using lattice Boltzmann-based single-phase model. J. Coll. Interf. Sci. **311**, 609–618 (2007)
18. Jia, X, McLaughlin, JB, Kontomaris, K: Lattice Boltzmann simulations of drop coalescence and chemical mixing. Physica A **362**, 62–67 (2006)
19. Wu, M, Cubaud, T, Ho, C: Scaling law in liquid drop coalescence driven by surface tension. Phys. Fluids **16**, 51–54 (2004)
20. Duchemin, L, Eggers, J, Josserand, C: Inviscid coalescence of drops. J. Fluid Mech. **487**, 167–180 (2003)
21. Colagrossi, A, Landrini, M: Numerical simulation of interfacial flows by smoothed particle hydrodynamics. J. Comput. Phys. **191**, 448–475 (2003)
22. Morris, JP: Simulating surface tension with smoothed particle hydrodynamics. Int. J. Numer. Meth. Fluids **33**, 333–353 (2000)
23. Hu, XY, Adams, NA: A multi-phase SPH method for macroscopic and mesoscopic flows. J. Comp. Phys. **213**, 844–861 (2006)
24. Adami, S, Hu, XY, Adams, NA: A conservative SPH method for surfactant dynamics. J. Comp. Phys. **229**, 1909–1926 (2010)
25. Hu, XY, Adams, NA: An incompressible multi-phase SPH method. J. Comp. Phys. **227**, 264–278 (2007)
26. Hu, XY, Adams, NA: A constant-density approach for incompressible multi-phase SPH. J. Comp. Phys. **228**, 2082–2091 (2009)
27. Adami, S, Hu, XY, Adams, NA: A new surface-tension formulation for multi-phase SPH using a reproducing divergence approximation. J. Comp. Phys. **229**, 5011–5021 (2010)
28. Acevedo-Malavé, A, García-Sucre, M: 3D coalescence collision of liquid drops using smoothed particle hydrodynamics. INTECH Publishers **5**, 85–106 (2011)
29. Acevedo-Malavé, A, García-Sucre, M: Head-on binary collisions of unequal size liquid drops with smoothed particle hydrodynamics. Transworld Research Network **9**, 245–266 (2012)
30. Acevedo-Malavé, A, García-Sucre, M: Coalescence collision of liquid drops I: off-center collisions of equal-size drops. AIP Adv. **1**(032117), 1–17 (2011)
31. Acevedo-Malavé, A, García-Sucre, M: Coalescence collision of liquid drops II: off-center collisions of unequal-size drops. AIP Adv. **1**(032118), 1–12 (2011)
32. Monaghan, JJ: Extrapolating B splines for interpolation. J. Comput. Phys. **60**, 253–262 (1985)
33. Lucy, LB: A numerical approach to the testing of the fission hypothesis. Astron. J. **82**, 1013–1024 (1977)
34. Gingold, RA, Monaghan, JJ: Smoothed particle hydrodynamics: theory and application to non-spherical stars. Roy Astronom Soc. **181**, 375–389 (1977)
35. Di Lisio, R, Grenier, E, Pulvirenti, M: The convergence of the SPH method. Computers Math. Applic. **35**, 95–102 (1998)
36. Bibette, J, Morse, DC, Witten, TA, Weitz, DA: Stability criteria for emulsions. Phys. Rev. Lett. **69**, 2439–2443 (1992)
37. Ivanov, IB, Dimitrov, DS: Thin Liquid Films Fundamentals and Applications. Marcel Dekker, New York (1988)
38. Ivanov, IB, Kralchevsky, PA: Stability of emulsions under equilibrium and dynamic conditions. Coll. Surf. A **128**, 155–175 (1997)
39. Kabalnov, A, Wennerström, H: Macroemulsion stability: the oriented wedge theory revisited. Langmuir **12**, 276–292 (1996)
40. Sharma, A, Ruckenstein, E: Stability, critical thickness, and the time of rupture of thinning foam and emulsion films. Langmuir **3**, 760–768 (1987)